Langmuir
Article
pubs.acs.org/Langmuir


# Nanoscale Patterning of Microtextured Surfaces to Control Superhydrophobic Robustness

Tae-Gon Cha,[†,‡] Jin Woo Yi,[§] Myoung-Woon Moon,*[,§] Kwang-Ryeol Lee,[§] and Ho-Young Kim*[,†]

[†]*School of Mechanical and Aerospace Engineering, Seoul National University, Seoul 151-744, Korea,* [‡]*School of Mechanical Engineering, Purdue University, West Lafayette, Indiana 47907, and* [§]*Future Fusion Technology Laboratory, Korea Institute of Science and Technology, Seoul 136-151, Korea*

*Received December 16, 2009. Revised Manuscript Received January 22, 2010*

Most naturally existing superhydrophobic surfaces have a dual roughness structure where the entire microtextured area is covered with nanoscale roughness. Despite numerous studies aiming to mimic the biological surfaces, there is a lack of understanding of the role of the nanostructure covering the entire surface. Here we measure and compare the nonwetting behavior of microscopically rough surfaces by changing the coverage of nanoroughness imposed on them. We test the surfaces covered with micropillars, with nanopillars, with partially dual roughness (where micropillar tops are decorated with nanopillars), and with entirely dual roughness and a real lotus leaf surface. It is found that the superhydrophobic robustness of the surface with entirely dual roughness, with respect to the increased liquid pressure caused by the drop evaporation and with respect to the sagging of the liquid meniscus due to increased micropillar spacing, is greatly enhanced compared to that of other surfaces. This is attributed to the nanoroughness on the pillar bases that keeps the bottom surface highly water-repellent. In particular, when a drop sits on the entirely dual surface with a very low micropillar density, the dramatic loss of hydrophobicity is prevented because a novel wetting state is achieved where the drop wets the micropillars while supported by the tips of the basal nanopillars.

## I. Introduction

There have been numerous studies on the creation of super-water-repellent surfaces to date. Although a patent on water-repellent materials dates back to the mid-20th century,[1,2] recent advances in micro- and nanofabrication technology triggered an increase in superhydrophobic surface research. Superhydrophobicity has been commonly characterized by the high contact angle of a surface with a water drop approaching 180° and the low tilt angle for the onset of drop rolling. In general, super-water-repellent surfaces support water drops on the tips of hydrophobic microscopic protrusions with the aid of air trapped in the roughness, and this situation is called the Cassie state.[3] However, additional measures of the quality of superhydrophobicity have recently attracted atttention,[4−6] especially when associated with the robustness of the water-repellent properties of surfaces. Lafuma and Quéré[4] pointed out that a robust superhydrophobic surface should be able to support water drops in the Cassie (or Fakir) state against increased interior pressure of the drop (that may be caused by squeezing the drop between plates or by reducing the drop size through evaporation) to push the meniscus into the gaps of microscopic protrusions. In this respect, increasing the aspect ratio of hydrophobic micropillars is reported to enhance the robustness of the superhydrophobic surfaces.[5]

An alternative route to enhancing superhydrophobicity has been suggested by forming hierarchical roughness on surfaces combining microscale and nanoscale textures. This was inspired by the structure of naturally existing superhydrophobic surfaces found in many living systems, including lotus leaves,[7] water strider legs,[8] gecko feet,[9,10] and insect wings.[11] Artificial hierarchical structures were reported where nanoasperities were formed on top of micropillars.[12−15] These surfaces exhibited a higher contact angle and lower contact angle hysteresis (the difference between the advancing and the receding contact angles) than the surfaces with single-roughness structures. However, the previous studies provide only a partial answer to why nature selects to have hierarchical surface structures: in actual lotus leaves, the entire surface is covered with nanoasperities, including the base area as well as the top of the microbumps. Artificially fabricated microtextured surfaces entirely decorated with nanoasperities were recently reported to increase the static contact angle.[16] It was shown that the density of micropillars could be dramatically reduced while maintaining the superhydrophobicity by covering the entire surface including the base area with nanoasperities.[6] Thus-prepared surfaces were shown to strongly resist the invasion of water drops into micropillar gaps when the drops were pressed onto them, but no quantitative assessment of the degree of resistance was addressed. Furthermore, there has been no quantitative measurement to compare the drop wetting behavior on a micropillar array entirely decorated with nanopillars, with the behavior on the surface partially covered with nanoroughness only at the micropillar tops.

Along with the comparison of artificial hierarchical surfaces with different nanotexture coverage, measuring the superhydrophobic

*Corresponding authors. E-mail: mwmoon@kist.re.kr, hyk@snu.ac.kr.

(1) Norton, F. J. U.S. Patent 2,386,259, Oct 9, **1945**.
(2) Gao, L.; McCarthy, T. J. *Langmuir* **2006**, *22*, 5998–6000.
(3) Cassie, A. B. D.; Baxter, S. *Trans. Faraday Soc.* **1944**, *40*, 546–550.
(4) Lafuma, A.; Quéré, D. *Nat. Mater.* **2003**, *2*, 457–460.
(5) Reyssat, M.; Yeomans, J. M.; Quéré, D. *Europhys. Lett.* **2008**, *81*, 26006.
(6) Kwon, Y.; Patankar, N.; Choi, J.; Lee, J. *Langmuir* **2009**, *25*, 6129–6136.
(7) Neinhuis, C.; Barthlott, W. *Ann. Bot.* **1997**, *79*, 667–677.
(8) Gao, X.; Jiang, L. *Nature* **2004**, *432*, 36.
(9) Hansen, W. R.; Autumn, K. *Proc. Natl. Acad. Sci. U.S.A.* **2005**, *102*, 385–389.
(10) Cho, W. K.; Choi, I. S. *Adv. Funct. Mater.* **2008**, *18*, 1089–1096.
(11) Byun, D.; Hong, J.; Saputra; Ko, J. H.; Lee, Y. J.; Park, H. C.; Byun, B.-K.; Lukes, J. R. *J. Bionic Eng.* **2009**, *6*, 63–70.
(12) Jeong, H. E.; Lee, S. H.; Kim, J. K.; Suh, K. Y. *Langmuir* **2006**, *22*, 1640–1645.
(13) Gao, X.; Yao, X.; Jiang, L. *Langmuir* **2007**, *23*, 48864891.
(14) Cortese, B.; D'Amone, S.; Manca, M.; Viola, I.; Cingolani, R.; Gigli, G. *Langmuir* **2008**, *24*, 2712–2718.
(15) Bhushan, B.; Koch, K.; Jung, Y. C. *Soft Matter* **2008**, *4*, 1799–1804.
(16) Lee, Y.; Park, S.-H.; Kim, K.-B.; Lee, J.-K. *Adv. Mater.* **2007**, *19*, 2330–2335.

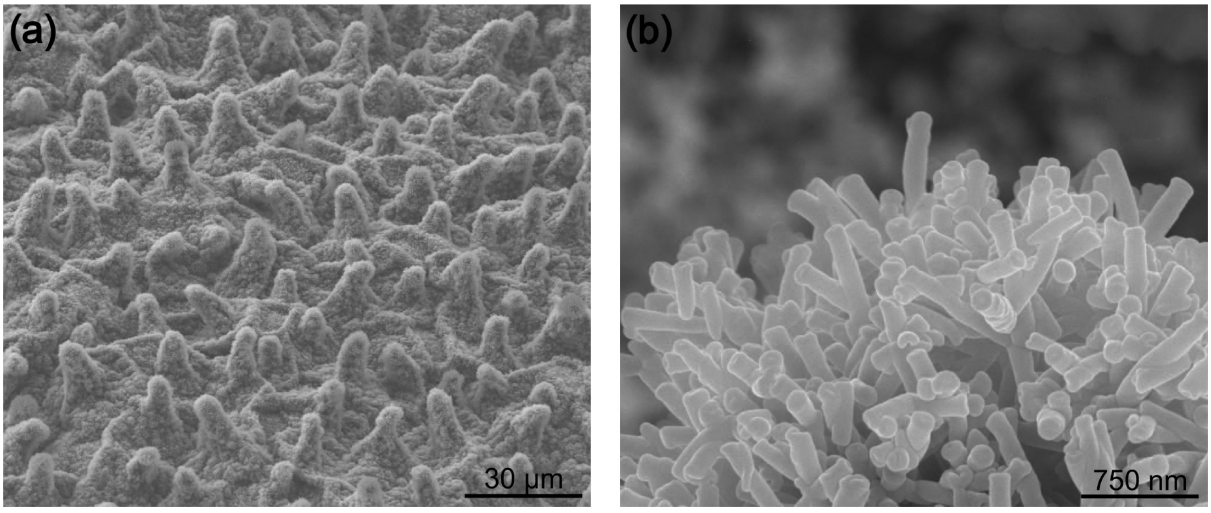


**Figure 1.** SEM images of a lotus leaf, *Nelumbo nucifera*. (a) The surface is covered with hierarchical roughness so that the microbumps and the basal area are entirely decorated with nanoprotrusions. (b) Randomly oriented nanocylinders that cover a microbump.

robustness of a real lotus leaf is of interest in this work. Although the static contact angle and the critical tilt angle for water drop rolling on a lotus leaf were reported previously,[17] the robustness of this natural hierarchical surface has seldom been considered. Such information would help us to evaluate the quality (in terms of robustness) of the water-repellent properties of artificial surfaces compared to those of natural ones.

From a theoretical point of view, Wenzel[18] and Cassie and Baxter[3] laid the framework for understanding the role of surface roughness in wettability. However, when hierarchical or dual structures are formed on surfaces, the wetting states of protrusions on the microscale and nanoscale may differ from each other.[12] For example, a water drop supported at the top of micropillars (Cassie state) may wet the nanostructure on the micropillar tops (Wenzel state). Although this issue was treated for the micropillar arrays covered on top with nanopillars,[12] the difference in wetting states due to the different coverage of nanotextures on micropillar arrays has not been addressed thus far. In particular, the quantitative assessment of the wetting-state evolution with the decrease in micropillar density (or the increase in pillar spacing) is important in understanding the role of nanotexture in superhydrophobic states, as will be clarified below.

In this work, we experimentally measure the wetting characteristics, with special emphasis on the robustness of superhydrophobicity, of different kinds of microscopic surface structures. To this end, we fabricate single-roughness surfaces on the microscale and nanoscale and dual-roughness surfaces with different nanotexture coverage (micropillar arrays partially covered on top with nanopillars only and arrays entirely covered on both tops and bases with nanopillars). Before addressing the superhydrophobic robustness of various surfaces with single and dual roughness, we first characterize the wetting behavior of the surfaces with nanoscale roughness by varying the nanotexture dimensions. Then we compare the robustness of the surfaces with different microscopic structures, including a natural lotus leaf, in terms of the degree of resistance against the increasing drop pressure that forces the liquid meniscus to wet the spaces between protrusions. Finally, we compare the evolution of the wetting states of water drops on those various surfaces as the micropillar density decreases to show the enhanced robustness of superhydrophobicity by nanostructuring the entire microtextured surface.

(17) Barthlott, W.; Neinhuis, C. *Planta* **1997**, *202*, 1–8.
(18) Wenzel, R. N. *Ind. Eng. Chem.* **1936**, *28*, 988–994.

## II. Materials and Methods

In the experiments, we investigated six different types of surfaces, one natural and five artificial. As a natural hydrophobic surface, we used a lotus leaf, *Nelumbo nucifera*. As artificial surfaces, we prepared bare silicon wafers, single-roughness surfaces with micropillar arrays, single-roughness surfaces with nanoscale pillars, hierarchical surfaces with micropillars decorated with nanoprotrusions only on their tops (surfaces with partial dual roughness), and hierarchical surfaces with nanoscale roughness on both micropillar tops and bases (surfaces with entirely dual roughness).

**A. Observation of a Lotus Leaf.** A lotus leaf, *Nelumbo nucifera*, collected from a local pond was cleaned with an air gun to remove dust particles. The leaf surface is covered with hydrophobic epicuticular wax crystals,[17] and its water repellency is enhanced by the intrinsic surface structure. The surface was observed with a scanning electron microscope (SEM, FEI-Nova NanoSEM 200). As shown in Figure 1, the surface is covered with microscale bumps, and the entire area, including bumps and bases, is decorated with randomly oriented nanopillars. The average diameter and height of the 15 representative microbumps are measured to be $8.6 \pm 2.3$ and $11.2 \pm 0.9$ $\mu$m, respectively. The average spacing between two adjacent bumps is $15.1 \pm 7.6$ $\mu$m. The cylindrical nanopillars are $118 \pm 6$ nm in diameter and $527 \pm 39$ nm in height, on average.

**B. Surfaces with Single Roughness.** To fabricate single-roughness surfaces with cylindrical micropillar arrays, deep reactive ion etching (DRIE) is employed. The pillar dimensions are selected such that they match those of microbumps found on the lotus leaf, thus the pillar diameter and height are 8 and 10 $\mu$m, respectively. We fabricate surfaces with various pillar spacings to investigate their effects, thus the pitch of a square array formed by the pillars varies between 10 and 100 $\mu$m.

To create nanoscale roughness on flat Si surfaces, Si(100) wafers are etched using rf glow discharge of $CF_4$ plasma using the PACVD (plasma-assisted chemical vapor deposition) method. The gas pressure and the bias voltage are maintained at 30 mTorr and $-600$ V, respectively. Nanopillar forests are created on the Si surface because of the local deposition of carbon films supplied by $CF_4$ gas and the preferred etching of exposed Si by F atoms,[19,20] which have a high reactivity with respect to Si.[21] The

(19) Kim, T.-Y.; Ingmar, B.; Bewilogua, K.; Oh, K. H.; Lee, K.-R. *Chem. Phys. Lett.* **2007**, *436*, 199–203.
(20) Zhao, Y.-P.; Dortar, J. T.; Wang, G.-C.; Lu, T.-M. *Phys. Rev. Lett.* **1999**, *82*, 4882–4885.
(21) Detter, X.; Palla, R.; Thomas-Boutherin, I.; Pargon, E.; Cunge, G.; Joubert, O.; Vallier, L. *J. Vac. Sci. Technol., B* **2003**, *21*, 2174–2183.

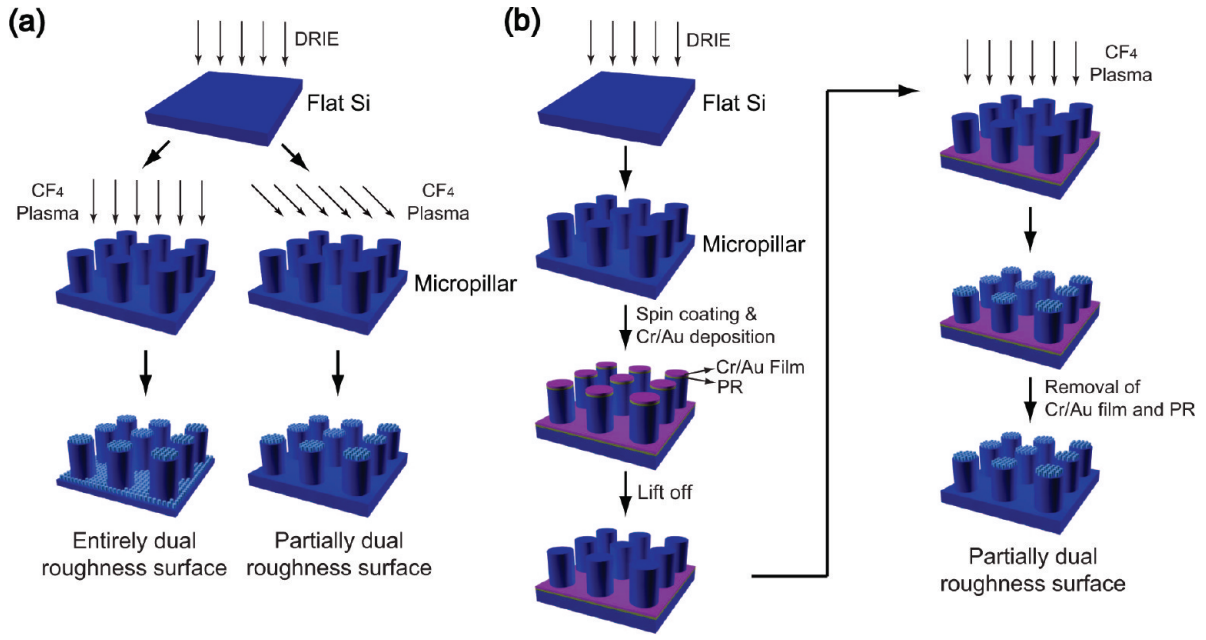


**Figure 2.** Fabrication process of dual-roughness surfaces. (a) Fabrication of the surface with dual roughness with the direct incidence of $CF_4$ plasma. (b) Fabrication of the surface with partially dual roughness via masking the basal area with a Cr/Au layer.

irradiation time of $CF_4$ plasma determines the height, the diameter, and the spacing of the nanopillars resulting from the etching. We vary the treatment time of flat Si surfaces between 10 and 60 min to investigate its effects on the surface morphology and the consequent wetting behavior. We selected the area of 3.5 × 3.5 $\mu m^2$ for measurements of the pillar dimensions through SEM.

**C. Surfaces with Dual Roughness.** Micropillars are formed first by the DRIE process on a Si wafer. Then $CF_4$ plasma etching imposes nanopillar forests on the microroughness surface. The process is schematically shown in Figure 2a. In this manner, both the base area and the pillar tops are decorated with nanoasperities, thus a surface with entirely dual roughness can be prepared.

To fabricate surfaces with partially dual roughness where only micropillar tops are nanotextured, two different methods are employed. As shown in Figure 2a, the oblique incidence of $CF_4$ plasma on micropillar arrays etches only the pillar tops while the base area is shaded by the pillars. This is owing to the straightness of the plasma beam that we use and is found to be effective unless the pillar spacing exceeds 10 $\mu$m.

For pillar spacing greater than 10 $\mu$m, we develop a novel method to mask the base area between micropillars while the pillar tops are exposed to $CF_4$ plasma, as shown in Figure 2b. During this process, we spin coat the whole surface with photoresist after micropillars are created by DRIE. Then Cr/Au films with a thickness of 200 nm are deposited on the photoresist layer using a lift dome device, and the Cr/Au films and photoresist layers on top of the micropillars are lifted off with acetone but the masking film on the base area is unaffected. After $CF_4$ plasma creates nanopillars only on top of micropillars, the Cr/Au films on the base area are removed by Cr and Au etchants for 20 min, respectively. After finally removing the bottom photoresist layer, we obtain a surface with partially dual roughness. It was found that Cr/Au films and the photoresist layer on the base can withstand $CF_4$ plasma treatment for up to 30 min. Thus, for experiments evaluateing the effects of micropillar spacing (ranging from 10 to 100 $\mu$m) on the superhydrophobic robustness, the tested surfaces with nanostructures are identically treated with $CF_4$ plasma for 30 min. Figure 3 shows the SEM images of all kinds of artificial surfaces fabricated in this work: surfaces with microscale single roughness, nanoscale single roughness, partially dual roughness, and entirely dual roughness.

**D. Lowering the Surface Energy.** To lower the surface energy of the foregoing surfaces with various morphology, an a-(C:H:Si:O) film is deposited on each surface using hexamethyldisiloxane (HMDSO) gas in the RF PACVD process.[22] Various bias voltages ranging from −100 to −800 V were tested to find the most hydrophobic coating conditions, revealing that the static contact angle of water on the flat Si surface was kept almost constant near 90° when the voltage ranged between −100 and −400 V. As the bias voltage exceeded −500 V, the contact angle started to decrease. The selected process condition in this work is such that the gas pressure is 10 mTorr, the bias voltage is −400 V, and the treatment time is 20 s. These conditions yield the static contact angle of water to be 91 ± 1° on the flat Si surface.

**E. Contact Angle Measurement.** The static contact angle of water on each surface is measured by taking and analyzing the images of sessile water drops with a volume of 2 $\mu$L with a CCD camera having a resolution of 1360 pixels × 1024 pixels. To measure the advancing contact angle, the volume of a sessile drop is slowly increased by a syringe pump at 1.2 $\mu$L/min. The critical advancing contact angle $\theta_A$ corresponds to the contact angle of the drop when its contact line (where the three phases of liquid−solid−gas meet) starts to move. The critical receding contact angle $\theta_R$ is measured when the contact line starts to recede as the drop volume decreases by evaporation. The contact angles were obtained by measuring the angle between the solid surface and the tangential line of a meniscus where it touches the solid. The contact angle hysteresis (CAH), a measure of the stickiness of a surface with water, is defined as $CAH = \theta_A - \theta_R$. All measurements were made at room temperature and a relative humidity of 35−55%.

## III. Results and Discussion

**A. Wettability of Nanotextured Surfaces.** Because the nonwettting behavior of single-roughness hydrophobic micropillar arrays was reported previously,[4,5,23] here we focus on the effects of the nanopillar morphology, controlled by $CF_4$ plasma

(22) Grischke, M.; Hieke, A.; Morgenweck, F.; Dimigen, H. *Diamond Relat. Mater.* **1998**, *7*, 454–458.
(23) Callies, M.; Chen, Y.; Marty, F.; Pépin, A.; Quéré, D. *Microelectron. Eng.* **2005**, *78*−*79*, 100–105.

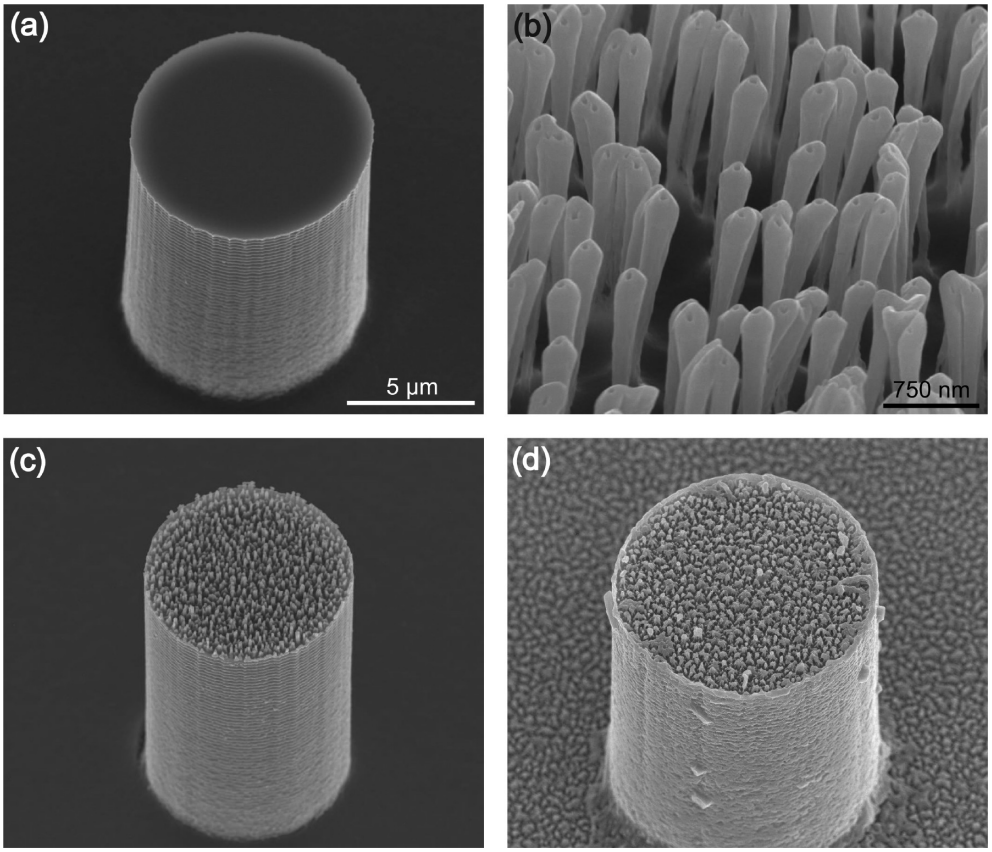


**Figure 3.** SEM images of the artificially prepared surfaces: surfaces with (a) microscale single roughness, (b) nanoscale single roughness, (c) partially dual roughness, and (d) entirely dual roughness. The magnifications in images a, c, and d are identical.

**Table 1. Dimensions of Nanopillars Varying with $CF_4$ Plasma Treatment Time**

| treatment time (min) | diameter (nm) | height (nm) | spacing (nm) |
|---|---|---|---|
| 10 | 42 ± 4 | 60 ± 3 | 98 ± 50 |
| 20 | 152 ± 11 | 245 ± 18 | 205 ± 104 |
| 30 | 179 ± 19 | 388 ± 23 | 261 ± 51 |
| 40 | 197 ± 16 | 480 ± 18 | 275 ± 139 |
| 50 | 227 ± 23 | 558 ± 27 | 321 ± 163 |
| 60 | 305 ± 36 | 861 ± 57 | 452 ± 229 |

treatment, upon the contact angle of water. Table 1 lists the diameter, the height, and the spacing of nanopillars formed on flat Si surfaces as varied by $CF_4$ plasma treatment time. The Table shows that as the treatment time $\tau$ increases, the nanopillars become wider (diameter $d$ increases) and taller (height $h$ increases) and the distance between the adjacent pillars, $s$, increases. To find the roughness $r$, defined as the ratio of the actual rough area to the projected area, and the solid fraction $f_s$, defined as the ratio of the cylindrical pillar top area to the projected area, we simply assume that the nanopillars form a square array[24] having a pitch of $s$. Then $r$ and $f_s$ are respectively calculated as

$$r = 1 + \frac{\pi dh}{(d+s)^2} \quad (1)$$

$$f_s = \frac{\pi^2}{4\left(1+\frac{s}{d}\right)^2} \quad (2)$$

(24) Choi, C.-H.; Kim, C.-J. *Phys. Rev. Lett.* **2006**, *96*, 066001.

Figure 4a shows that the roughness monotonically increases with the plasma treatment time. However, the solid fraction is the lowest for the shortest treatment time, $\tau = 10$ min, and reaches its maximum at $\tau = 20$ min. Then $f_s$ tends to decrease with further increases in $\tau$.

The measurement results of the static contact angle ($\theta_s$) and the contact angle hysteresis (CAH) are shown in Figure 4b together with the theoretical contact angle values assuming the wetting states of Cassie and Wenzel. The configurations of the drop interfaces in those states are illustrated in Figure 5a,b. In the Cassie and Wenzel states, $\theta_s$ is given respectively by $\cos\theta_s = -1 + f_s(1 + \cos\theta_0)$ and $\cos\theta_s = r\cos\theta_0$, where $\theta_0$ is the static contact angle of the flat surface, 91°. The measured contact angles approach the theoretical predictions based on the Cassie formula, and they match almost perfectly when $\tau = 60$ min. The discrepancy between the measured and theoretical contact angles indicates that the drop is not at the perfect Cassie state on the surface treated with plasma for $\tau < 50$ min. In particular, the fact that the measured contact angle for $\tau = 10$ min is neither as high as the corresponding theoretical value nor larger than other contact angles obtained by longer treatment time, despite the smallest $f_s$, indicates a severe degree of water invasion into the nanoroughness on this surface. Figure 4b shows that CAH decreases with treatment time from 46 ± 3 to 15 ± 3°. Callies et al.[23] observed with superhydrophobic micropillar arrays of single roughness that CAH decreases with the decrease in the solid fraction, consistent with our experimental results with nanotextured surfaces except for the case of $\tau = 10$ min. Additional mechanism to lower CAH in our nanosurfaces with increased $\tau$ may involve the increased pillar height and spacing, which makes the Cassie state more robust. It should be noted that unlike

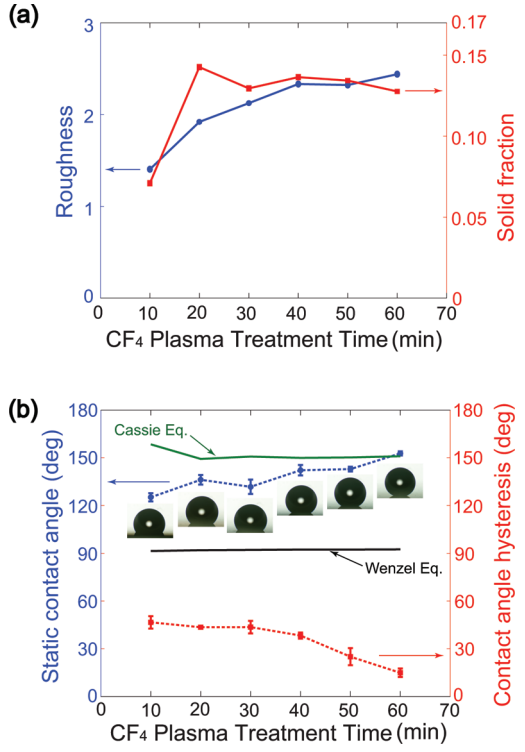


**Figure 4.** Effects of the $CF_4$ plasma treatment time on (a) the surface morphology (roughness and solid fraction) and on (b) the wettability ($\theta_s$ and CAH).

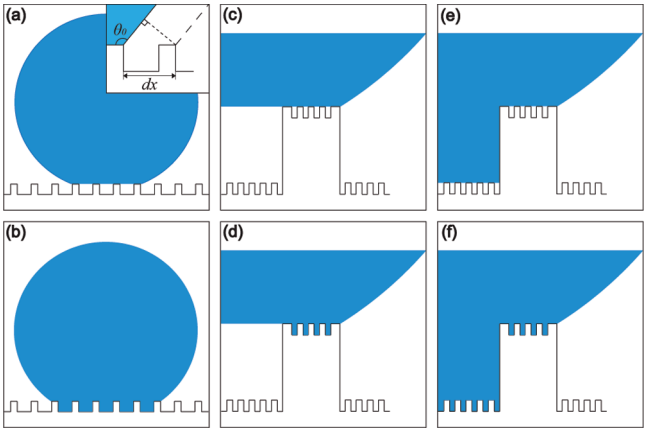


**Figure 5.** Interface configurations on rough surfaces in different wetting states: (a) Cassie state., (b) Wenzel state, (c) Cassie−Cassie state, (d) Cassie−Wenzel state, (e) Wenzel−Cassie state and (f) Wenzel−Wenzel state.

micropillar arrays the depth of nanopillar forests is only tens to hundreds of nanometers, thus the separation of the water−air interface from the bottom surface (required for the Cassie state) may become imperfect. The surface that is plasma treated for 10 min has only 60 nm in pillar height, thus it is very probable that the drop is in the mixed state of those of Wenzel and Cassie. This explains the low contact angle and the high CAH despite the lowest $f_s$ of this surface relative to those of the other nanoscale single-roughness surfaces that are treated with plasma for longer durations.

**B. Drop Pressure and Superhydrophobic Robustness.** When millimetric water drops with a volume of 2 $\mu$L are placed on the various surfaces prepared in this work, all of the microscopically rough surfaces exhibited strongly hydrophobic

**Table 2. Static Contact Angles of Water Drops on Different Types of Microscopically Rough Surfaces**

| surface | microscale single roughness | nanoscale single roughness | partially dual roughness | entirely dual roughness |
|---|---|---|---|---|
| $\theta_s$ | 143° | 149° | 144° | 150° |

character, possessing static contact angles greater than 140°. See Table 2. For the surface with microscale single roughness and the surface with dual roughness, we use a micropillar spacing of 10 $\mu$m for comparison with a lotus leaf having similar microbump spacing. Thus, the nanotextures on the surface with partially dual roughness are formed by the oblique incidence of $CF_4$ plasma for 60 min. We measure the evolution of the receding contact angle versus the evaporation rate, defined as the time normalized by the total evaporation time. The initially high contact angles do not persist because the sessile drops shrink because of evaporation,[5] as shown in Figure 6.

The interior pressure of a drop relative to the surrounding gas is given by the Laplace pressure $\Delta P = 2\gamma/R$, where $\gamma$ is the surface tension of the liquid and $R$ is the radius of a drop with a spherical cap shape. As $R$ decreases because of evaporation, $\Delta P$ increases and liquid can be forced into asperities to collapse air pockets that support the drop. In the simplistic scenario where the drop could choose only either the perfect Cassie state or the perfect Wenzel state, the contact angle would abruptly decrease from the high value corresponding to the Cassie state to the low value of the Wenzel state. However, the actual measurement results reveal that the contact angle decrease is gradual rather than abrupt on the superhydrophobic surfaces used in this work.

On the hydrophobized flat Si surface, the contact angle starts to decrease immediately with evaporation. It is noted that because of contact line pinning the contact angle decreases almost to zero. However, on the superhydrophobic surfaces, the Cassie state is maintained in the initial stages, thus the reduction of the high contact angle is much milder than that on the flat Si surface. The Figure shows that a dramatic decrease in the contact angle from 146 to 120° is observed for the surface with nanoscale single roughness when the evaporation rate reaches 19%. This signals the departure of the wetting state from the Cassie state. Unlike the surface with nanoscale single roughness, the other superhydrophobic surfaces exhibit no such sudden descent of the contact angle. This is considered to be because the region of the Wenzel state slowly replaces that of the Cassie state on those surfaces. The surface with microscale single roughness maintains a higher contact angle than the surface with nanoscale single roughness when the evaporation rate ranges between 0.19 and 0.5, which is attributed to the greater pillar height that impedes the transition to the Wenzel state.[25] The contact angles on surfaces with dual roughness, both natural and artificial, are maintained at high values even longer than the surfaces with single roughness. Among the surfaces with dual roughness, the partially dual surface loses its high contact angle earlier than the natural and the artificial entirely dual surfaces. Considering that the top surfaces of micropillars of the two kinds of artificial dual surfaces are identically decorated by nanopillars, the difference in the contact angle evolution directly reflects the impact of bottom roughness on the wetting behavior. As illustrated in Figure 7a, on the partially dual surface, the liquid forced into micropillars wets the bottom surface relatively easily. (Recalled that the static contact angle of the hydrophobized smooth Si surface is 91°.)

(25) Kusumaatmaja, H.; Blow, M. L.; Dupuis, A.; Yeomans, J. M. *Europhys. Lett.* **2008**, *81*, 36003.

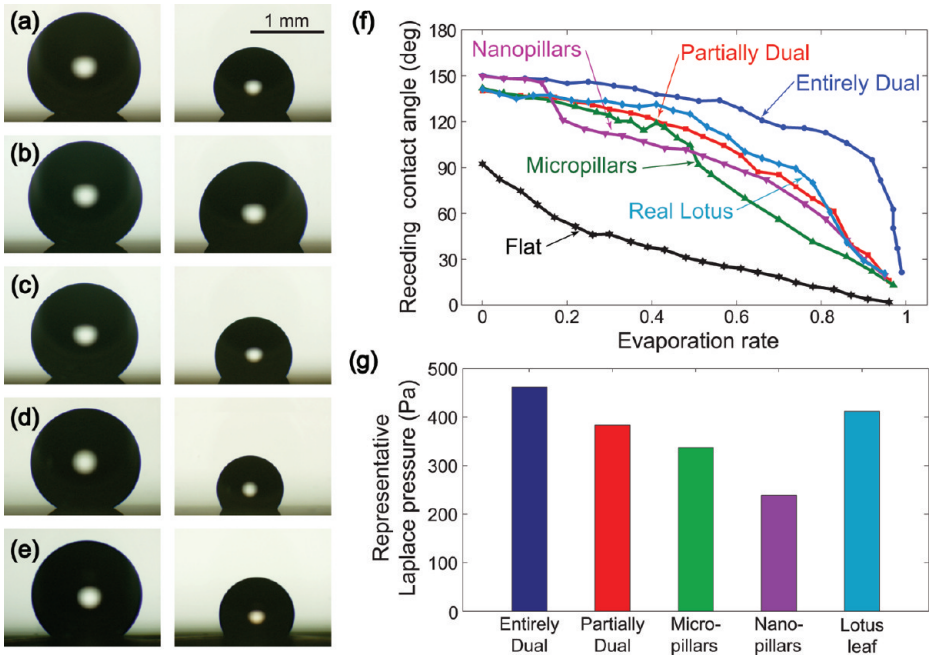


**Figure 6.** Robustness of superhydrophobic surfaces against the increased drop pressure caused by evaporation. The images of water drops in the beginning of the experiment and when the receding contact angle reaches 120° are shown on (a) the surface with microscale single roughness, (b) the surface with nanoscale single roughness, (c) the partially dual surface, (d) the entirely dual surface, and (e) the real lotus leaf. (f) Evolution of the contact angle with evaporation on the different types of surfaces. (g) The representative Laplace pressure that each superhydrophobic surface can endure until the receding contact angle reaches 120°.

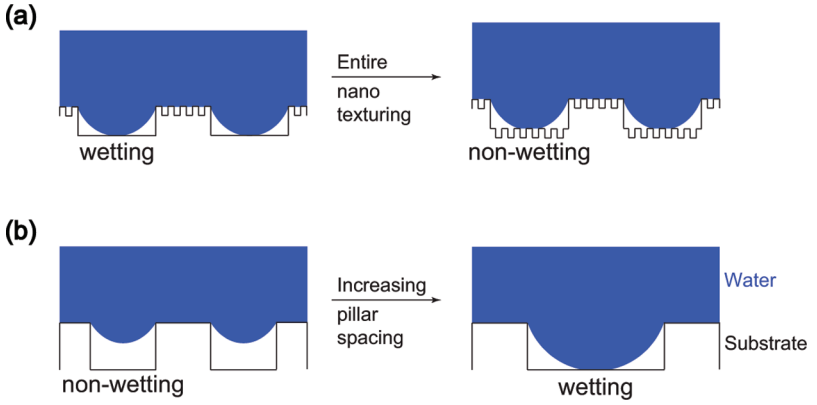


**Figure 7.** Profiles of a meniscus hanging from micropillars. (a) Resistance of the basal nanotexture to wetting. (b) Sagging of the meniscus with increased pillar spacing that causes the wetting of the bottom.

However, on the entirely dual surface, the forced liquid encounters additional superhydrophobic basal nanostructures, thus the wetting of the bottom area is strongly resisted.

The contact angle on the lotus leaf is maintained at a higher value than that on the artificial partially dual surface but lower than that on the artificial entirely dual surface. The nanostructures covering the entire lotus leaf including the microbumps and the base explain the enhanced nonwetting behavior (or superhydrophobic robustness) relative to that on the partially dual surface. The difference of the superhydrophobic robustness of the lotus leaf from that of the artificial entirely dual surface is considered to arise primarily from the directionality of the nanopillars. The randomly packed nanopillars on the lotus leaf (Figure 1b) make contact with a water drop over a greater area than the artificially prepared, highly oriented straight nanopillars (Figure 3b). Therefore, the artificial nanostructure is superior to the natural nanostructure in terms of the water-repellent strength. We see that the artificially prepared surface with entirely dual roughness maintains the high contact angle for the longest time during evaporation.

To quantitatively compare the observations plotted in Figure 6f, we calculate the Laplace pressure of a drop on each superhydrophobic surface when the contact angle reaches 120°, corresponding to the value signaling the failure of the Cassie state for the surface with nanoscale single roughness. This can be considered to be the representative interior pressure of a drop that each surface can endure before losing its superhydrophobicity, and the results are shown in Figure 6g. The value is the lowest for the surface with nanoscale single roughness having the shortest pillars, and it increases in the following order: the surface with microscale single roughness, the partially dual surface, the lotus leaf, and the entirely dual surface. In particular, the entirely dual surface resists a Laplace pressure that is 26% higher than on the partially dual surface, clearly showing that nanostructuring the entire microtextured surface enhances the robustness of the superhydrophobicity against the increased interior pressure of a drop.

**C. Micropillar Density and Superhydrophobic Robustness.** The foregoing experiments reveal the enhanced resistance of the entirely dual surface to wetting as a result of decreased drop size as compared to that for surfaces with partially dual and single roughness. Now we evaluate the effects of nanostructuring the entire surface area on the robustness of the superhydrophobic state as the micropillar density varies. The aforementioned formula for the static contact angle of a drop in the Cassie state implies that $\theta_s$ increases with increased micropillar spacing or decreased micropillar density, $f_s$. However, the excessive reduction of the pillar density causes the liquid−air interface that is sagging between the distant microposts to touch the bottom surface[25] as illustrated in Figure 7b, thus the Cassie state can no longer be maintained.

Before describing the experimental results of measuring $\theta_s$ with the varying micropillar density, we give a theoretical consideration of the wetting states of dual-roughness surfaces. To adequately describe the contact mode of a drop sitting on a surface with two different length scales of roughness, a separate consideration of the contact mode of the liquid with micropillars and with nanopillars should be made. Depending on the contact mode, the equilibrium contact angle can be theoretically given considering the energy variation associated with the infinitesimal displacement of the contact line. When a drop wets neither micro- nor nanoasperities but sits on the tips of both structures as shown in Figure 5c, it is said to be in the Cassie−Cassie state. In this case, the free-energy change, d$E$, due to the displacement of the contact line, d$x$, is given by

$$\frac{dE}{dx} = -\cos(\pi - \theta_{CC})\gamma + (1 - f_{SM}f_{SN})\gamma + f_{SM}f_{SN}(\gamma_{SL} - \gamma_{SG}) \quad (3)$$

where $\theta_{CC}$ is the apparent contact angle of the Cassie−Cassie state, $f_{SM}$ and $f_{SN}$ are the fractions of the liquid contact area with microroughness and nanoroughness, respectively, and $\gamma_{SL}$ and $\gamma_{SG}$ are the interfacial energies of solid/liquid and solid/gas, respectively. Using Young's equation, $\gamma \cos\theta_0 = \gamma_{SG} - \gamma_{SL}$, and the energy-minimum principle, $dE/dx = 0$, $\theta_{CC}$ is determined as

$$\cos\theta_{CC} = f_{SM}f_{SN}(\cos\theta_0 + 1) - 1 \quad (4)$$

For the Cassie−Wenzel mode, where the drop is suspended on the micropillars but wets the nanopillars as shown in Figure 5d, $dE/dx$ is written as

$$\frac{dE}{dx} = -\cos(\pi - \theta_{CW})\gamma + (1 - f_{SM})\gamma + f_{SM}r_N(\gamma_{SL} - \gamma_{SG}) \quad (5)$$

where $\theta_{CW}$ is the apparent contact angle of the Cassie−Wenzel state and $r_N$ is the roughness factor of the nanopillars. Then we get

$$\cos\theta_{CW} = f_{SM}(r_N\cos\theta_0 + 1) - 1 \quad (6)$$

In the Wenzel−Cassie mode, where the micropillars are wet but the nanopillars still support the liquid drop as shown in Figure 5e, we write $dE/dx$ as

$$\frac{dE}{dx} = -\cos(\pi - \theta_{WC})\gamma + (1 - f_{SN})\gamma + (r_M - f_{SN} - 1)(\gamma_{SL} - \gamma_{SG}) \quad (7)$$

where $\theta_{WC}$ is the apparent contact angle of the Wenzel−Cassie state and $r_M$ is the roughness factor of the micropillars. Then the contact angle in this mode is given by

$$\cos\theta_{WC} = (f_{SN} - 1 + r_M)\cos\theta_0 + f_{SN} - 1 \quad (8)$$

When both the microscale and nanoscale roughnesses are wet as shown in Figure 5f, the system is in the Wenzel−Wenzel state and the energy change becomes

$$\frac{dE}{dx} = -\cos(\pi - \theta_{WW})\gamma + (r_M + r_N - 1)(\gamma_{SL} - \gamma_{SG}) \quad (9)$$

The corresponding contact angle $\theta_{WW}$ satisfies

$$\cos\theta_{WW} = (r_M + r_N - 1)\cos\theta_0 \quad (10)$$

As mentioned earlier, in the experiments to evaluate the effect of the micropillar density, we created nanopillars with 30 min of $CF_4$ plasma treatment. Then the corresponding $f_{SN}$ and $r_N$ values are measured to be 0.367 and 4.19, respectively.

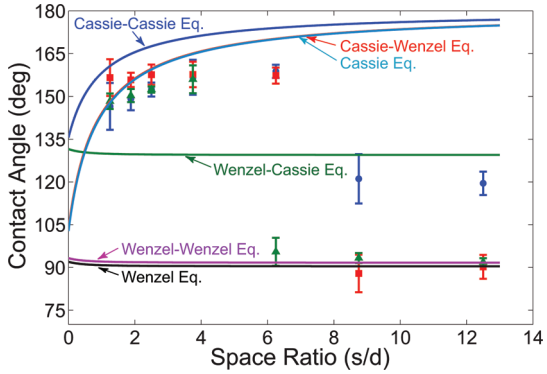


**Figure 8.** Static contact angle of water drops on surfaces with varying micropillar density. The solid lines correspond to the theoretical predictions for each wetting state. The green triangles denote the experimentally measured contact angle on the surface with microscale single roughness, the red squares denote the contact angle on the partially dual surface, and the blue circles denote the contact angle on the entirely dual surface.

Figure 8 shows the experimentally measured and theoretically predicted contact angles of the surface with microscale single roughness, the partially dual surface, and the entirely dual surface while increasing the space ratio of the micropillar array defined as $s/d$. On the surface with microscale single roughness, the Cassie state is maintained for the relatively high micropillar densities until the space ratio reaches 4. When the space ratio exceeds 6, the contact angle drops to that of the Wenzel state, indicating that the micropillars and the bottom become wet. For the drop on the partially dual surface, comparing the experimentally measured contact angles and theoretical predictions reveals that the micropillars support the drop and the nanopillars are wet for low space ratios corresponding to the Cassie−Wenzel state. This observation is consistent with the results reported by Jeong et al.,[12] who used polymeric partially dual pillar structures. The high contact angle of our partially dual surface is maintained until the space ratio reaches 6, at which the foregoing surface with microscale single roughness fails to keep the Cassie state, owing to the elevated energy barrier to completely wet the dual rough surface. However, when the space ratio exceeds 8, the drop finally wets the bottom area entering the Wenzel−Wenzel state.

When the surface with entirely dual roughness is tested, high contact angles are attained until the space ratio reaches 6, indicating the prevalence of the Cassie−Wenzel state. As the

space ratio exceeds 8, the contact angle suddenly drops, as does the partially dual surface at the same ratio. This makes physical sense because the upper structures of the micropillars are identical for the partially dual and the entirely dual surfaces. However, it is remarkable that the amount of contact angle reduction is much smaller for the entirely dual surface. Instead of dropping to the angle corresponding to the Wenzel−Wenzel state (∼90°), the contact angle assumes a value close to 120°. Comparing this value with the theoretical predictions reveals that the system is in the Wenzel−Cassie state. Although the micropillars are wet because of increased pillar spacing, the nanostructured bottom area still supports the water drop, preventing the entire dominance of the Wenzel state. The Wenzel−Cassie state continues to be at work when the space ratio reaches 12.5. This clearly shows the enhanced superhydrophobic robustness of the entirely dual roughness surface against the dilution of micropillars. We note that the sessile liquid drop in the Wenzel−Cassie state is both experimentally achieved and theoretically matched for the first time to our knowledge.

## IV. Conclusions

Although the surfaces with dual roughness have been shown to possess superior superhydrophobicity compared to the surfaces with single roughness, the role of nanotexture coverage on the microstructured surfaces has not been fully addressed thus far. Therefore, we studied the effects of nanotexture coverage on the robustness of superhydrophobicity by comparing the water-repellent properties of the surfaces with microscale single roughness, with nanoscale single roughness, with partially dual roughness, and with entirely dual roughness. As the first step in understanding the role of nanostructure, we evaluated the effects of nanopillar dimensions of the single-roughness surface on the degree of water repellency. Then we measured the contact angle of evaporating water drops on differently textured surfaces to find that the entirely dual surface endures the highest interior pressure of the drop before losing its superhydrophobicity. The natural lotus leaf was revealed to have stronger water repellency than the partially dual surface but to lose its high contact angle earlier than the entirely dual surface because of the random orientation of the nanopillars. Last, by changing the micropillar density, we found that the surface with entirely dual roughness maintains a relatively high static contact angle at an extremely dilute micropillar distribution by preventing the wetting of the bottom surface.

The observations of the enhanced robustness of the entirely dual surface against the increased drop interior pressure and meniscus sagging are attributed to the nanoroughness on the micropillar base, which keeps the bottom surface very water-repellent. Our work can help in better understanding the role of nanostructures in naturally found and artificially created hierarchical superhydrophobic surfaces and also in fabricating more robust surfaces with strong water repellency.

**Acknowledgment.** This work was supported by the National Research Foundation of Korea through grant no. 2009-0067974 and by the Ministry of Knowledge Economy of Korea through the Fundamental R&D Program for Core Technology of Materials. H.-Y.K. acknowledges the administrative support of the SNU Engineering Research Institute.